Iranian Journal of Electrical and Electronic Engineering

Journal Homepage: ijeee.iust.ac.ir

Research Paper

An Improved Sensorless Rotor Position Computation for Integrated Direct Power and Vector Control of S-VSC Interfaced DFIG

R. Kalyan*, M. Venkatakirthiga*(C.A.), and P. Raja*

Abstract: The Direct power control and vector control of DFIG has known advantages, but certain disadvantages like steady state performance and transient performance of the system still persist. In order to overcome these, a novel technique based on Improved Sensorless Rotor Position Computational Algorithm with Integrated Direct Power and Vector Control (IDPVC) for S-VSC interfaced DFIG is proposed in this work. The advantages of both vector control and direct power control techniques are addressed in this method. This proposed IDPVC control minimizes the real and reactive power ripples at steady state and total harmonic distortion in stator current. In the proposed control, data acquired from sensorless rotor position computation makes the system more stable and avoids the sensor maintenance and feedback errors. The proposed system is tested for a 3.73 kW DFIG and compared with a benchmark DPC control of single VSC based DFIG. The results show the effectiveness of the approach under various wind speed conditions and found to be satisfactory.

Keywords: Voltage Source Converter, Sensorless Rotor Position, Vector Control, Direct Power Control.

Nomenclature

V_a, V_b	Stator phase voltages, V
i_a, i_b	Stator phase currents, A
i_{ra}, i_{rb}	Rotor phase currents, A
$V_{s\alpha}, V_{s\beta}, i_{s\alpha}, i_{s\beta}$	α and β components of voltages and currents, V and A
P_S, Q_S	Stator real and reactive powers at stator terminals, W
P_S^{ref}, Q_S^{ref}	Reference stator real and reactive powers, W
P_E, Q_E	Errors obtained from Real and reactive power, W
$I_{dr}^{ref}, I_{qr}^{ref}$	Reference rotor dq-axes currents, A
I_{dr}, I_{qr}	Obtained rotor dq-axes currents
$i_{r\alpha}, i_{r\beta}$	αβ currents, A
I_{drE}, I_{qrE}	Errors from actual and reference rotor dq-axes currents , A
I_{dhb}, I_{qhb}	Hysteresis bands for controllers
S_{dr}, S_{qr}	Switching states from hysteresis controllers
$\psi_{s\alpha}, \psi_{s\beta}$	Stator αβ flux linkages,
$I_{crowbar}$	Current in crow bar resistance
$sin\,\mu,\ cos\,\mu$	Stator magnetizing angle vectors
ω_e	Stator angular velocity, rad/s
$i_{r\alpha}^s, i_{r\beta}^s$	rotor currents in stator RF, A
$cos\,\hat{\theta}_C, sin\ \hat{\theta}_C$	Computed slip angle vectors
i_{dr}^r, i_{qr}^r	Rotor currents in rotor RF
ψ_s^r	Stator flux in rotor RF
N	Sector location
P_W	Wind power, W
P_B	Battery power, W
R_S, R_r	Stator and rotor resistance, Ω
L_S, L_r	Stator and rotor inductance, H
L_m	Mutual inductance, H
J	Rotational moment of inertia, kg-m^2
D	Frictional coefficient

Iranian Journal of Electrical and Electronic Engineering, 2023. Paper first received 01 Jun 2022, revised 28 Mar 2023, and accepted 15 Apr 2023.

*The authors are National Institute of Technology Tiruchirappalli, Trichy, India.

E-mails: kalyankali@gmail.com, mvkirthiga@nitt.edu and praja@nitt.edu.

Corresponding Author: M. Venkatakirthiga.

https://doi.org/10.22068/IJEEE.19.2.2546.

1 Introduction

OWING to the rising energy demand, environmental risks and degradation of fossil fuels renewable energy sources are being the main focus in the recent past to cater the needs of

future expansion [1]. Renewable Energy Sources (RES) are fulfilling the electricity demand of remote and islanded communities. The clean energy from these sources impact less the public health system, and also helps to reduce energy cost as they require very little maintenance [2]. Among many renewable energy sources, solar and wind energy systems are the major sources for pollution free environment. Earlier, wind energy systems were limited to hilly areas and high-speed wind areas but, due to recent development in WEECS, they are used for localised environment too such as roads, spacious parks etc.

Among various wind energy conversion topologies, DFIGs are the most effective power generation schemes in order to cope with the uncertainty in wind speeds and reduced capacity power converter at the machine side [3]. Earlier, majority of wind energy was being generated through the fixed speed wind turbines coupled with squirrel cage induction generators [4]. Gradually later on, variable speed turbines were used to extract more energy from the wind and reduce noise compared to fixed speed wind turbines [5-8]. Due to the recent advancements in the power electronic controllers the complexity in wind power control is also minimized. In many earlier works, Field-oriented control (FOC) is used for independent control of real and reactive power for the conventional DFIG. However, FOC is more complex and involves more transformations [9-11]. To overcome the difficulties of FOC direct power control has been introduced. DPC controls both real and reactive power with good dynamic response without any complex transformations [12]. Later, many researchers started to focused on sensorless rotor position estimation to avoid delayed signals, and reduced design complexity.

Subsequently, most power engineers focused on encoder less computations for both vector and direct power control of real and reactive powers in the conventional DFIG control topologies [13-19]. E. Bogalecka has used rotor flux calculation for the control of active and reactive power, resulting in low frequency harmonics in rotor currents near synchronous speed [13]. Datta et al. proposed a method for rotor position estimation. This method has been used for direct power control and FOC control [14-15]. However, the calculation of magnetizing current is cumbersome. The model reference adaptive system (MRAS) for estimating the rotor position [16-17]. Slip position estimator is proposed in FOC for power control of DFIG. The estimator connected to PI controller in the algorithm is non-linear and gives oscillations in the output [18]. A computational algorithm for rotor position to generate the slip angles for the FOC control of convention DFIG, has been explained in [19]. Single VSC based DFIG was later adopted for the control of real and reactive power, to eliminate the grid side VSC. Battery has been used in support of reactive power and voltage [20]. Later, B. Singh et al. proposed independent direct power control technique to control active and reactive power in a hybrid DFIG system [21]. This technique gives good dynamic response. However, it involves complex calculations for the rotor position estimation. B. Singh et al. presented a single VSC DFIG with vector control by using model reference adaptive system for the rotor position [22]. R. M. Prasad et al. estimated rotor position based on reduced sensor and modified algorithm for the vector control of single VSC tied DFIG. This control technique employed three sensors for rotor position estimation but needs complex calculation [23]. R. M. Prasad et al. have attempted rotor power control through single VSC for DFIG based energy evacuation scheme. In this configuration, the DFIG rotor power is controlled and the rotor had connection with grid terminals [24]. New rotor position algorithms such as RPSA-II and I had been used for the direct power control of rotor tied DFIG [25]. Kalyan et al. have proposed a co-ordinated controller for the control of grid and battery power with single VSC based DFIG [26]. H.choja et.al proposed an artificial neural network based DPC control of DFIG is attempted to minimize the torque ripples [27]. In [28], B.Hu et al. have performed the analysis of high frequency resonance and reshaped the control of DPC. S. Mondal et.al have presented a performance of reactive power controller strategy with active power damping with DTC control using matrix converter for DFIG [29]. The benefits of both the direct power control and vector control have been introduced for the better dynamic and steady state response of the conventional DFIG topology [30]. In this context, this research work proposes an integrated direct power and vector control (IDPVC) for S-VSC interfaced DFIG with sensor less rotor position (SLRP) computation. It has simple control structure, and it gives good transient and steady state response. Sensor less computation needs lesser computation, good tracking of real power reference with MPPT and adjustable power factor with respect to reference reactive power.

In the literature, the control of real and reactive power is performed for the conventional

DFIG/Single VSC DFIG and the position of rotor is calculated using sensor /sensorless algorithms. The proposed work integrates the vector and direct power control of single VSC based grid connected DFIG with sensorless rotor position computation (SLRPC). The control with single VSC DFIG is new with sensor less rotor position computation and analysed many parameters which improves the performance the system.

The hysteresis control with DFIG has good transient response but, the steady state real and reactive ripples are more [21]. From the literature, the vector control of DFIG give good steady state response but poor in transient response. The proposed IDPVC control has both the advantages to improve the performance of system.

The proposed IDPVC (integrated direct power and vector control) control has lesser steady-state ripples in real and reactive power and the stator currents has lesser THD when compared to the DPC (direct power control) as shown in results section 5. The proposed IDPVC control also shows the grid variations (LVRT) for the single VSC topology as per Indian electricity grid code (IEGC) standards and it effectively controls the performance parameters of the system shown in section 5.1

The manuscript is organized as follows: section 2 presents proposed system configuration for S-VSC interfaced DFIG, following introduction in section 1; Section 3 delineates the proposed control topology of IDPVC controlled S-VSC interfaced DFIG; SLRP computation for rotor position is articulated in section 4; sections 5 and 6 present the results and the comparison of proposed IDPVC control with SLRP computation with bench mark DPC control followed by conclusive remarks.

2 Proposed System Configuration of S-VSC-interfaced DFIG

The proposed grid connected IDPVC control of S-VSC interfaced DFIG with SLRP computation is shown in Fig. 1. It consists of DFIG which is directly connected to grid and rotor terminal is connected to a voltage source converter. The voltage source converter is connected to the battery used for voltage and reactive power support for the system. The configuration eliminates the grid side converter such that the system cost gets reduced.

The integrated control scheme is a combination of vector control (VC) and direct power control (DPC) which improves the performance by adding the advantages of both the methods, such that the transient response is improved by DPC control and steady response by vector control. By adding the VC control to the direct power control of single VSC DFIG the performance at steady state is improved and additionally SLRP computation eliminates the encoder for the system and further improves performance of the system.

The proposed IDPVC control with S-VSC DFIG incorporating MPPT operation of wind turbine gives smooth variations in stator real power and reactive power fed to the grid.

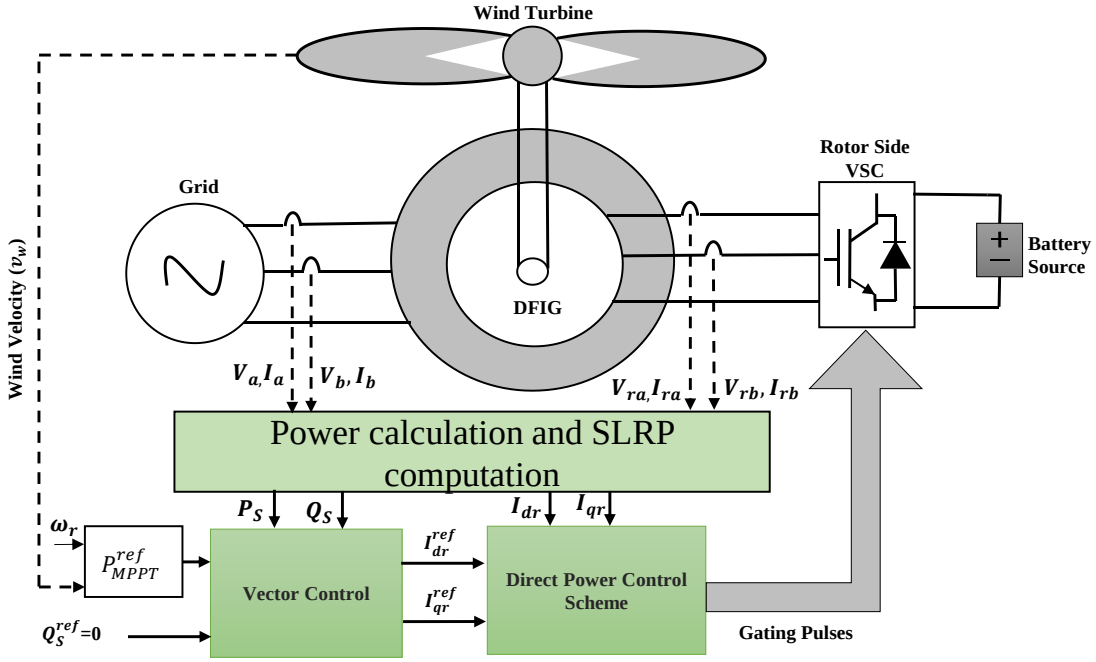

Fig. 1 System configuration for S-VSC interfaced DFIG.

3 Proposed Control Topology of S-VSC DFIG

In this proposed control scheme, the real and reactive powers are controlled by two PI controllers which produce reference rotor dq-axes currents (I_{dr}^{ref} ,I_{qr}^{ref}) as shown in Fig. 2. The errors (P_E, Q_E) for PI controllers are obtained from reference real and reactive power (P_S^{ref},Q_S^{ref}) and actual real and reactive powers (P_S, Q_S) respectively. Reference real power (P_S^{ref}) is obtained from MPPT of wind turbine and reference reactive power is selected as zero to obtain unity power factor.

The actual real and reactive powers are calculated from αβ voltages ($V_{s\alpha}$,$V_{s\beta}$) and currents ($i_{s\alpha}$, $i_{s\beta}$) as follows:

$$P_S = 2/3\left(v_{s\alpha}i_{s\alpha} + v_{s\beta}i_{s\beta}\right), Q_S = 2/3\left(v_{s\beta}i_{s\alpha} - v_{s\alpha}i_{s\beta}\right) \quad (1)$$

where stator αβ voltages and currents are calculated as:

$$v_{s\alpha} = \frac{3}{2}V_a,\ \ v_{s\beta} = \frac{\sqrt{3}}{2}(V_a, +2V_b)$$
$$i_{s\alpha} = \frac{3}{2}i_a,\ \ i_{s\beta} = \frac{\sqrt{3}}{2}(i_a, +2i_b) \quad (2)$$

The real and reactive power errors are computed as:

$$P_E = P_S^{ref} - P_S,\ Q_E = Q_S^{ref} - Q_S \quad (3)$$

The PI controllers compute the reference dq-axes rotor currents (I_{dr}^{ref} ,I_{qr}^{ref}) and the actual (I_{dr}, I_{qr}) currents obtained from combination of rotor αβ currents ($i_{r\alpha}$, $i_{r\beta}$) and computed angles from SLRP computation. The rotor current is computed as:

$$i_{dr}^r + j\, i_{qr}^r = (i_{r\alpha}^r + j\, i_{r\beta}^r)(cos\ \hat{\theta}_C - j\ sin\ \hat{\theta}_C) \quad (4)$$

where:

$$cos\ \hat{\theta}_C = cos\ \mu\ cos\ \theta_C + sin\ \mu\ sin\ \theta_C$$
$$sin\ \hat{\theta}_C = sin\ \mu\ cos\ \theta_C - cos\ \mu\ sin\ \theta_C \quad (5)$$

The errors from comparators of dq-axes currents (I_{drE}, I_{qrE}) are given to hysteresis controllers which generate switching states (S_{dr}, S_{qr}). The hysteresis bands (I_{dhb} *and* I_{qhb}) for controllers are shown in Fig. 3.

The switching states for hysteresis controllers are computed as follows:

$$S_{dr} = 1, \quad \forall\ I_{drE} > I_{dhb}$$
$$S_{dr} = -1, \quad \forall\ I_{drE} < -I_{dhb}$$
$$S_{dr} = 0, \forall\ -I_{dhb} < I_{drE} < I_{dhb} \quad (6)$$

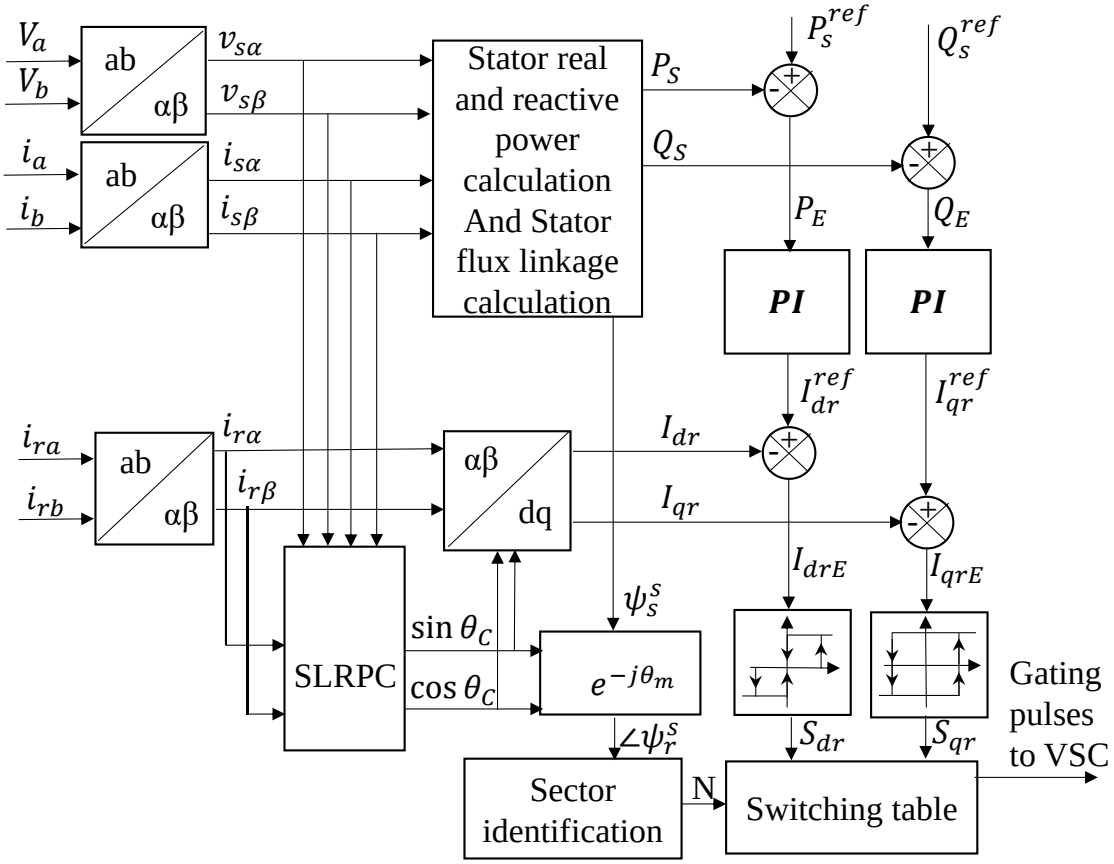

Fig. 2 IDPVC controlled S-VSC interfaced DFIG.

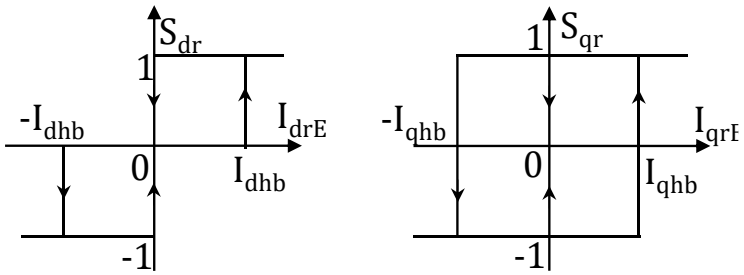

(a) (b)

Fig. 3 Hysteresis controllers for rotor dq-axes currents: (a) 3-level and (b) 2-level.

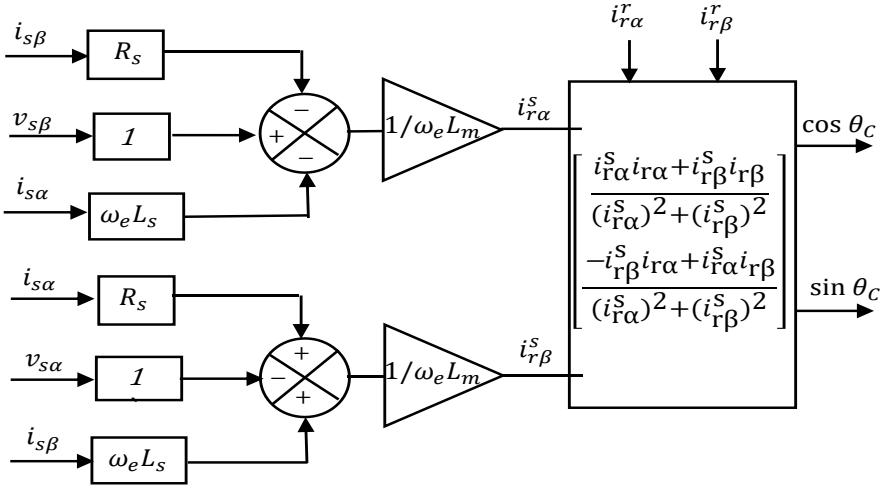

Fig. 4 SLRP computation for rotor position.

$$S_{qr} = 1, \quad \forall\, I_{qrE} > I_{qhb}$$
$$S_{qr} = -1, \quad \forall\, I_{qrE} < -I_{qhb} \tag{7}$$

The switching states and sector location (N) generate the voltage pulses for the converter

4 Sensorless Rotor Position Computation

Computation of rotor position required for IDPVC control is obtained from stator voltages, stator currents and rotor currents as shown in Fig. 4. The stator α and β quantities are obtained from Eq. (2), and the rotor currents ($i_{r\alpha}, i_{r\beta}$) are calculated as:

$$i_{r\alpha} = \frac{3}{2} i_{ra},\ i_{r\beta} = \frac{\sqrt{3}}{2}(i_{ra} + 2i_{rb}) \tag{8}$$

According to reference frame theory, the rotor position computed using stator voltages, current and rotor current are shown in Fig. 5. The stator voltage (V_S) is aligned with q-axis i.e., $V_S = V_{qs}$ and $V_{ds} = 0$. The stator flux linkages in stator Reference Frame (RF) are given as

$$\psi_{s\alpha}=L_s i_{s\alpha}+L_m i_{r\alpha}\,, \qquad \psi_{s\beta}=L_s i_{s\beta}+L_m i_{r\beta} \tag{9}$$

Here, the Eq. (9) constitutes two unknown parameters such as stator flux linkages ($\psi_{s\alpha}, \psi_{s\beta}$)and rotor currents ($i_{r\alpha}, i_{r\beta}$). The stator voltage equations are used to estimate the stator flux linkages which are written as:

$$v_{s\alpha} = R_s i_{s\alpha} + \frac{d}{dt}\psi_{s\alpha}, \qquad v_{s\beta} = R_s i_{s\beta} + \frac{d}{dt}\psi_{s\beta} \tag{10}$$

From the Fig. 5, stator flux in synchronous RF is written as:

$$\psi_{s\alpha} = |\psi_s| cos\ \mu, \quad \psi_{s\beta} = |\psi_s| sin\ \mu \tag{11}$$

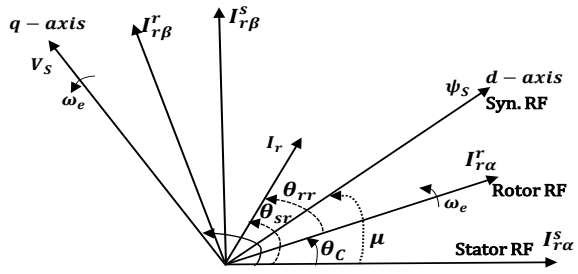

Fig. 5 Reference frame analogy for SLRP computation.

The stator flux linkages and magnetizing angle (μ) are functions of time which are differentiated as:

$$\frac{d}{dt}\psi_{s\alpha} = \frac{d}{dt}|\psi_s| sin\ \mu - \psi_{s\beta}\omega_e \tag{12}$$

$$\frac{d}{dt}\psi_{s\beta} = \frac{d}{dt}|\psi_s| cos\ \mu + \psi_{s\alpha}\omega_e \tag{13}$$

The differential terms with resultant stator flux are negligible in Eqs. (10) and (11) and the angular frequency represented as $\omega_e = \frac{d\mu}{dt}$ and substituting above equations in Eqs. (7) and (8) gives the simplified stator (α, β) voltage equations which are written as:

$$v_{s\alpha} = R_s i_{s\alpha} - L_s i_{s\beta}\omega_e - L_m i_{r\beta}\omega_e \quad (14)$$

$$v_{s\beta} = R_s i_{s\beta} + L_s i_{s\alpha}\omega_e + L_m i_{r\alpha}\omega_e \quad (15)$$

The rotor currents in stator RF are calculated as:

$$i^s_{r\alpha} = v_{s\beta} - R_s i_{s\beta} - L_s i_{s\alpha}\omega_e / L_m\omega_e \quad (16)$$

$$i^s_{r\beta} = R_s i_{s\alpha} - v_{s\alpha} + L_s i_{s\beta}\omega_e / L_m\omega_e \quad (17)$$

The stator angles $(sin\ \mu, cos\ \mu)$and angular velocity $(\omega_e)$are calculated as:

$$v_{s\alpha} = -\frac{V_a}{\sqrt{V_a^2 + V_b^2}}, v_{s\beta} = \frac{V_b}{\sqrt{V_a^2 + V_b^2}} \quad (18)$$

$$\omega_e = cos\ \mu \frac{d}{dt} sin\ \mu - sin\ \mu \frac{d}{dt} cos\ \mu \quad (19)$$

From the Fig. 5 the rotor currents from rotor RF is calculated as:

$$i^r_{r\alpha} + j\ i^r_{r\beta} = (i^s_{r\alpha} + j\ i^s_{r\beta}) e^{j(\theta_c)} \quad (20)$$

where $\theta_c = \theta_{sr} - \theta_{rr}$, and the slip angle vectors are computed as:

$$\begin{bmatrix} cos\ \theta_c \\ sin\ \theta_c \end{bmatrix} = \begin{bmatrix} \frac{i^s_{r\alpha} i^r_{r\alpha} + i^s_{r\beta} i^r_{r\beta}}{(i^s_{r\alpha})^2 + (i^s_{r\beta})^2} \\ \frac{-i^s_{r\beta} i^r_{r\alpha} + i^s_{r\alpha} i^r_{r\beta}}{(i^s_{r\alpha})^2 + (i^s_{r\beta})^2} \end{bmatrix} \quad (21)$$

The stator flux in rotor RF is computed as:

$$\psi^r_s = (\psi_{s\alpha} + j\ \psi_{s\beta})(cos\ \theta_c + j\ sin\ \theta_c) \quad (22)$$

where:

$$\psi_{s\alpha} = \int v_{s\alpha} - R_s\ i_{s\alpha},\ \psi_{s\beta} = \int v_{s\beta} - R_s i_{s\beta} \quad (23)$$

The position obtained from stator flux in rotor RF decides the sector location (N) and the associated switching states are used for the generation of gating pulses for the rotor tied VSC. The gating pulses are represented as $V_0(000) - V_7(111)$ which are six active vectors $(V_1 - V_6)$ and two null vectors $(V_0\ and\ V_7)$ shown in Fig. 6. The binary digits represent the ON/OFF states for top switches of VSC such as '0' represents OFF and '1' represents ON and complimented for bottom switches of VSC which are shown in Table 1. Consider the ψ_{sr} angle is obtained from the sensorless rotor position algorithm which decides the sector location say S_1 and switching states (S_{dr} & S_{qr}) from the controllers from the Eqs. (4) and (5), are considered as 1, 1 (such as dq-axes rotor current errors (I_{drE} & I_{qrE}) are more than the hysteresis bands (I_{dhb} & I_{qhb}). The S1 is the sector angle in the space vector shown in Fig. 7. To minimize the error according to space vector the V_5 is the voltage pulse fed to the converter then the error decreases and then V_6 pulse according to the switching state and then sector location gives the respective gating pulses for the converter.

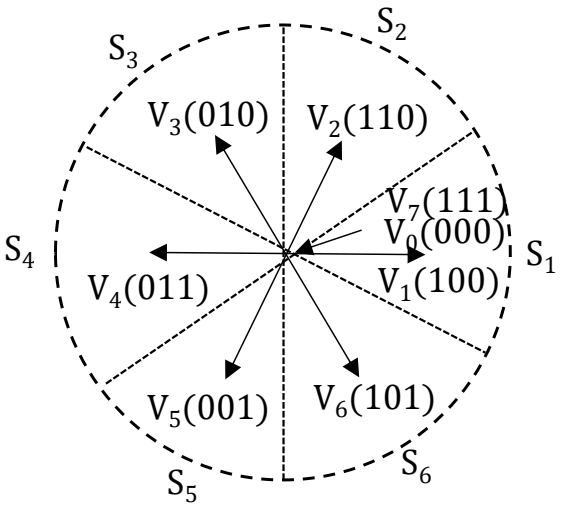

Fig. 6 Selection of sector location.

Table1 Gating pulses for the rotor tied VSC (switching table in Fig. 2)

S_{qr}	S_{dr}	S_1	S_2	S_3	S_4	S_5	S_6
1	1	V_5	V_6	V_1	V_2	V_3	V_4
	0	V_7	V_7	V_7	V_7	V_7	V_7
	-1	V_3	V_4	V_5	V_6	V_1	V_2
-1	1	V_6	V_1	V_2	V_3	V_4	V_5
	0	V_7	V_7	V_7	V_7	V_7	V_7
	-1	V_2	V_3	V_4	V_5	V_6	V_1

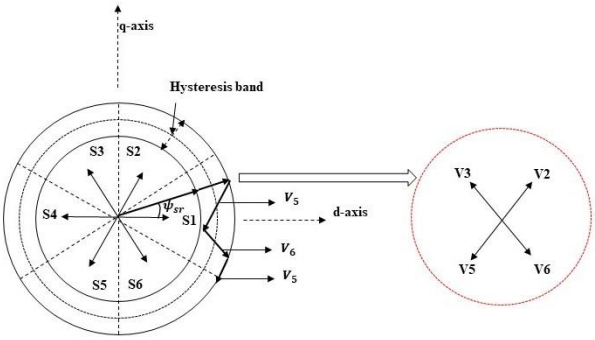

Fig. 7 Derived gating pulses shown in Table 1.

5 Results and Discussions

The proposed IDPVC control scheme with S-VSC interfaced DIFG depicted in Fig.2, is simulated in MATLAB/Simulink. To validate the performance of the proposed IDPVC technique, DFIG is made to operate at sub-synchronous (7 m/s), synchronous speed (9.85 m/s) and super synchronous speed (12 m/s) respectively.

Performance metrics in the form of sector location (N), calculated $(sin\ \theta)$ and computed $(sin\ \theta_C)$ slip angle vector which are obtained from DFIG rotor angle and proposed SLRP algorithm

respectively. These are evaluated for all the aforementioned speeds (sub- synchronous, synchronous, super- synchronous and dynamic variations) to test the efficacy of proposed IDPVC control with SLRP Computation.

The location of the sector and switching states decides the gating pulse variations for VSC which in turn results in DFIG stator power control. The sector region (N) is rotating from S_1 to S_6 (as shown in Fig. 6) in clock wise direction for sub synchronous speed, same sector is upheld as the previous state in synchronous speed and rotates in anti-clock wise direction (from S_6 to S_1) at super synchronous speeds. All the aforementioned three sectors are observed in dynamic conditions in the form of stepped waveforms viz-o-viz and clearly depicted in Fig. 8. A key point is observed that, slip angle vectors are tracked at same values irrespective of abrupt wind speed variations.

The dynamic performance of the controller is validated through change in speed conditions, through the three speed variations. The corresponding DFIG rotor speeds are 0.76 pu, 1.0 p.u and 1.18 p.u respectively. The observed parameters are rotor speed along with the (I_{Sabc}), and rotor current (I_{rabc}). The wind turbine is set to operate for sudden change in speeds in the from 7 m/s to 9.85 m/s and then it holds maximum up to 12 m/s. The corresponding stator and rotor currents, are shown in Fig. 9.

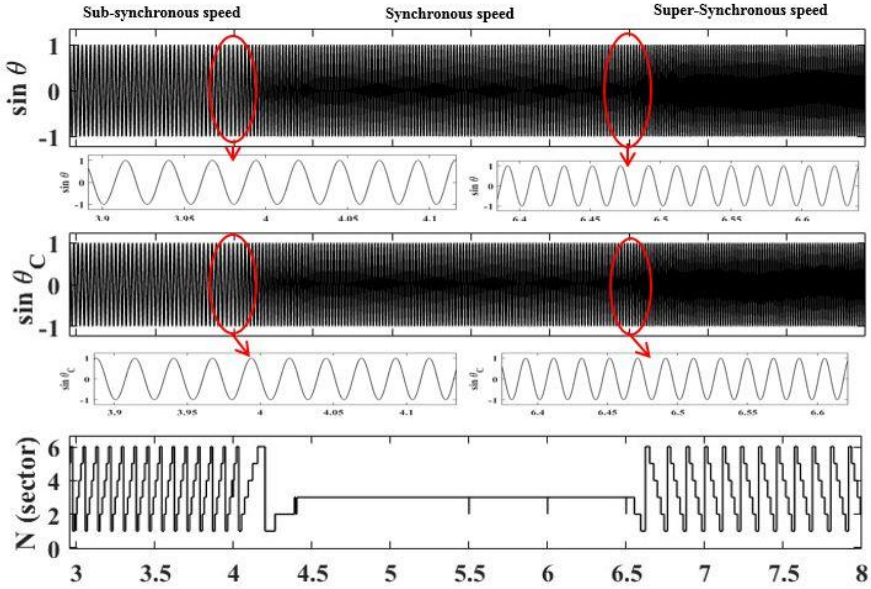

Fig. 8 The actual and computed slip angle vector, and sector location for 7m/s, 9.85m/s and 12m/s wind speed conditions.

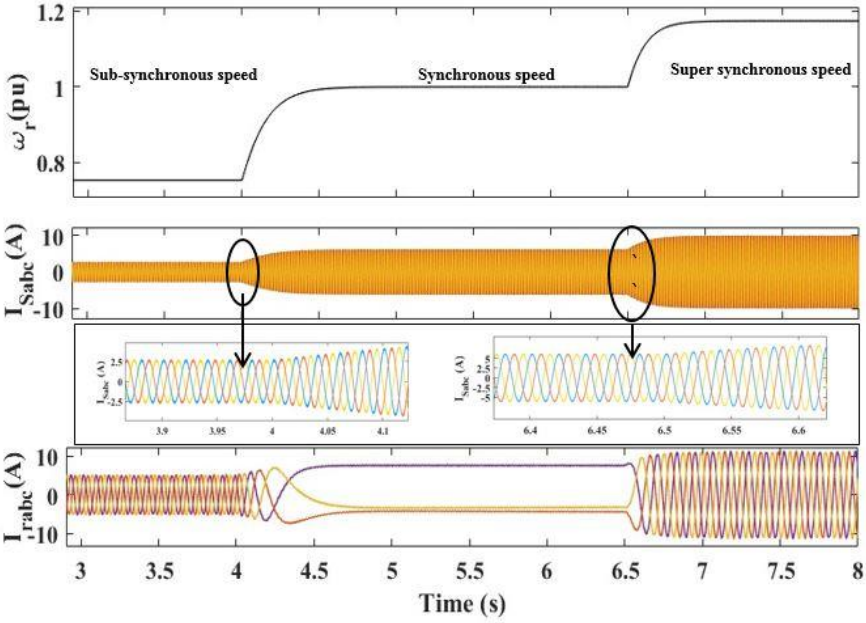

Fig. 9 The rotor speed, Stator currents, and rotor currents for 7m/s, 9.85m/s and 12m/s wind speed conditions.

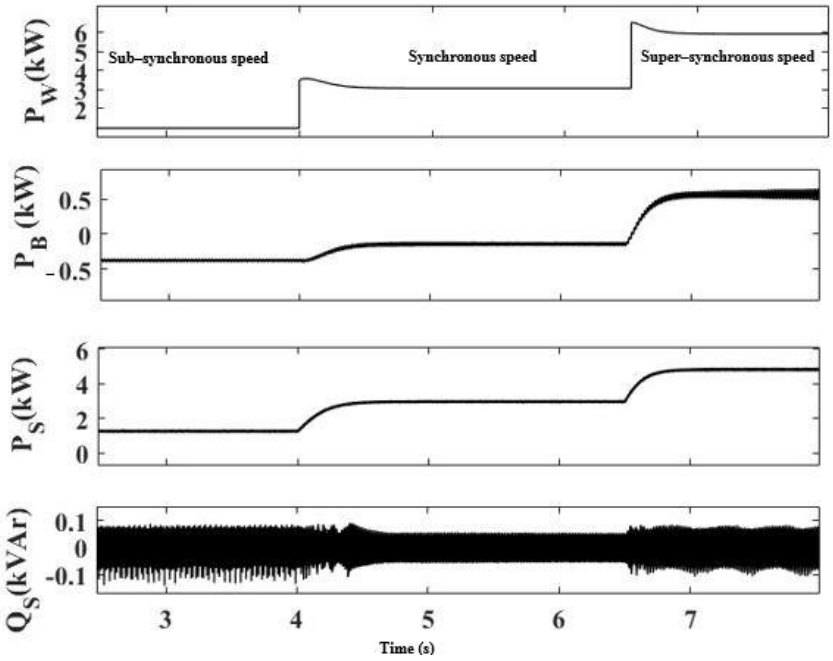

Fig. 10 Various power parameters for the proposed IDPVC control for 7m/s, 9.85m/s and 12m/s wind speed conditions.

Nevertheless, it is also observed that rotor currents in sub-synchronous speed, the flow of current is observed from the converter to the rotor which is vice-versa in super-synchronous speed. Positive sign convention represents, the former and the negative sign represents the latter, clearly observed in Fig. 9.

Key performance parameters like, wind power (P_W), battery power (P_B), stator real and reactive power (P_S) and stator reactive power (Q_S) for several wind speed conditions. Fig. 10 shows the dynamic performance for sub-synchronous, synchronous and super-synchronous conditions respectively for proposed IDPVC control with SLRP computation.

The wind power of 0.96kW is extracted at speed of 7 m/s, which is not alone sufficient to feed a grid with generated DFIG stator power. Therefore, the battery supports the grid with required deficit power of 0.35kW through the rotor side VSC. These two cumulatively maintain the required stator active power to track the reference value and maintain the reactive power to zero.

During synchronous speed conditions, wind power of 3.07 kW is extracted, which is sufficient enough to feed the grid with the DFIG generated power of 3kW, here battery is in floating condition i.e., neither charges nor discharges. Nonetheless, a small amount of power (0.11kW) is produced to feed the losses of the converter and machine.

At super synchronous speed of 12 m/s, wind turbine extracts power of 5.92kW and when the speed changed from synchronous speed to super synchronous speed, associated DFIG stator reference power is incremented from 3kW to 4.82kW which is more than the desired value. The excess power is fed to the battery, which makes the battery to be in the charging mode.

The proposed IDPVC technique results in smooth variations in real power and minimizes the fluctuations in both real and reactive power with sudden change in speed. In addition, the charging and discharging behavior of battery is also observed in Fig. 10

It is also observed that, the dq-axes rotor reference currents obtained from PI controllers and it is tracked by actual dq-axes rotor currents computed using SLRP algorithm shown in Fig. 11 and the dynamics of rotor dq-axes currents shown for various speed conditions. The Errors from the rotor currents feed to hysteresis controllers, which generates the switching states (as shown in Fig. 3). These are plays an important role for generation of voltage pulses for the VSC. The hysteresis bands for controllers are 0.42% of rated currents.

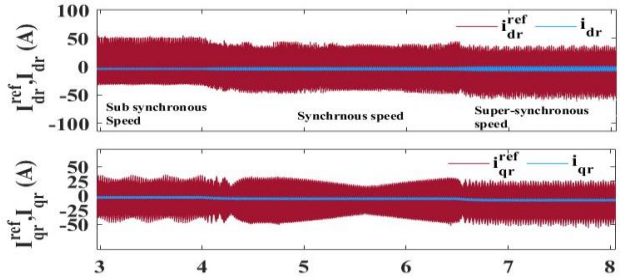

Fig. 11 Reference and actual dq-axes rotor currents (I_{dq}^{ref}, I_{dq}).

5.1 Proposed Control Analyzed under Grid Voltage Variations

The proposed topology under grid voltage variations is shown in section 5.1. As per Indian electricity grid code (IEGC) standards, the low-voltage ride-through operation as the system is shown in Figure 12. In this, the voltage dip is considered for 15% of the rated voltage as per IEGC [31-32].

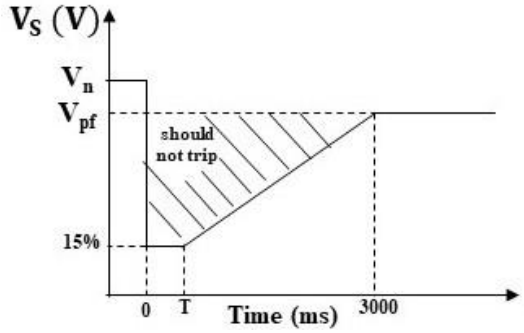

Fig. 12 LVRT standards (IEGC).

Here, V_n is the nominal voltage, V_{pf} is 80% of the nominal voltage, and T is the fault clearing time depending upon the nominal voltage level of machines mentioned by IEGC. In the shaded region, the machine should not trip so that the wind turbine could connect to the grid.

The proposed control topology with grid voltage variations of low voltage ride through (LVRT) and the parameters which effects by the grid variations are stator voltage (V_S), stator current (I_S), rotor currents (I_r), stator real power (P_S), stator reactive power(Q_S), battery power (P_B),crowbar current ($I_{crowbar}$), rotor speed(ω_r) as shown in Fig. 13. The machine is operated for a wind velocity of 12m/s is considered and the LVRT occurred at the time span of 3 s to 3.5 s and voltage is reduced to 15% of rated voltage. The crowbar is activated for 3 s to 3.1 s and the corresponding crowbar current is shown in Fig.13. At 3.5s the voltage increased in steps of 15pu and reach its rated value by 3.92 s. At 3 s the grid power is reduced to the minimum power of 600 W to meet losses and also to avoid the raise in rotor speed and currents of the stator and rotor. At 3.7 s the rated power is recovered and the system comes to normal condition.

6 Comparison and Validation of Results

The proposed grid connected IDPVC control of S-VSC DFIG with SLRP algorithm focuses on three important parameters which are fed to the grid such as stator current (I_{Sabc}), stator real power (P_S) and stator reactive power (Q_S). The performance proposed IDPVC control is compared with DPC control operated for various speed conditions.

The performance of proposed control improved in terms of stator real power fluctuations at steady state shown in Fig. 14. The magnitude of fluctuations is high with DPC control and the proposed IDPVC control reduces the magnitude of fluctuation and improves the quality of power fed to the grid. The performance of proposed IDPVC control with SLRP algorithm is operated for various speed conditions such as sub-synchronous (7 m/s), synchronous speed (9.85 m/s) and super synchronous speed (12 m/s) respectively.

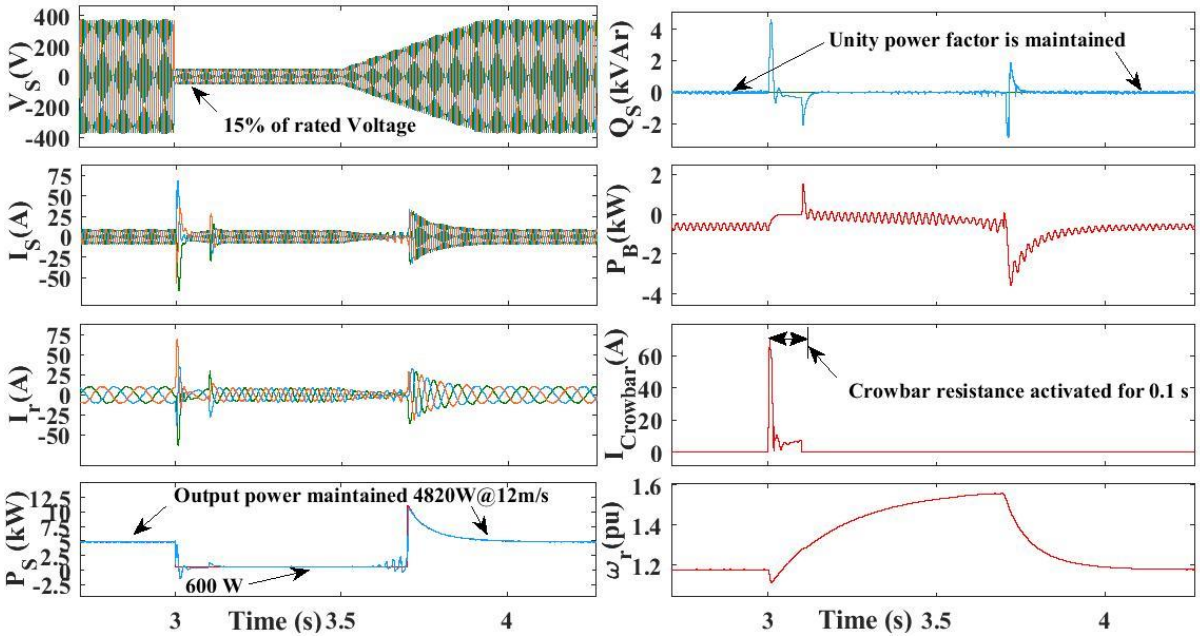

Fig. 13 Performance of proposed system with grid voltage variations occurred at 3s to 3.7s.

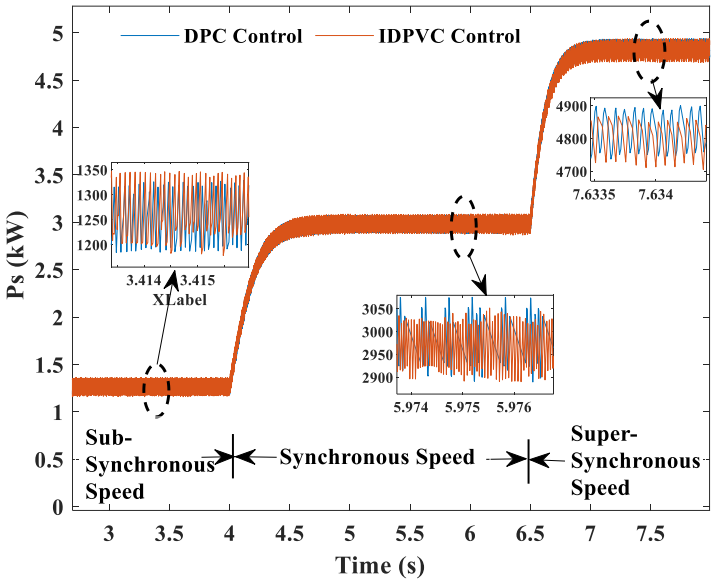

Fig. 14 Real power fluctuations in various speed conditions.

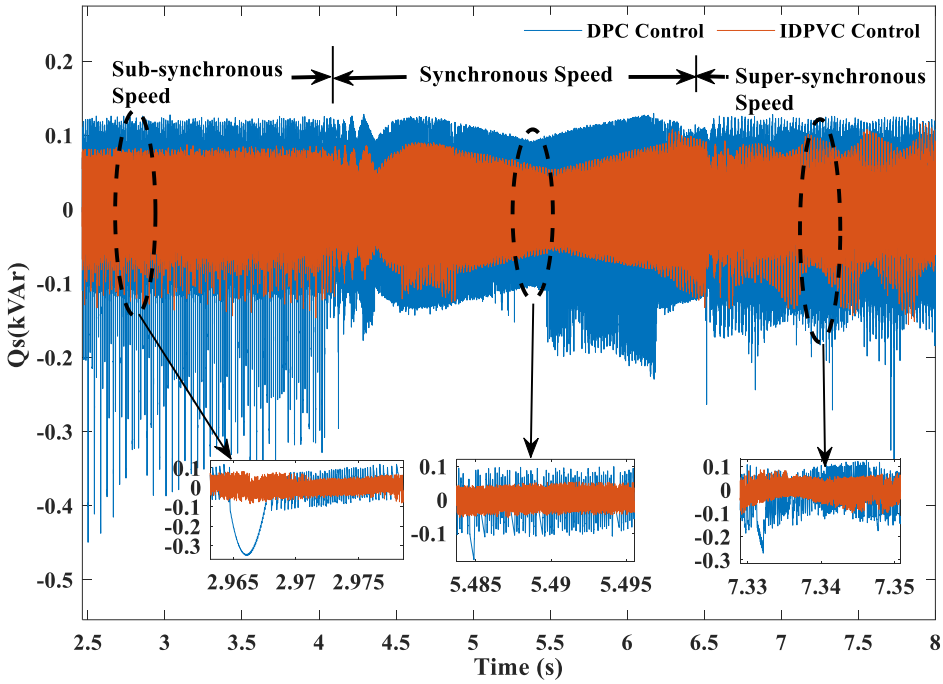

Fig. 15 Reactive power fluctautions in various speed condition.

At the sub-synchronous speed for a wind velocity of 7 m/s, the DFIG operated for up to 4sec and the steady state flctuations shown at instant of 3.414 to 3.415 seconds. At synchronous peed for a wind velocity of 9.85 m/s, the DFIG operated for 4 to 6.5 secs and the flacuataions shown at instant of 5.974 to 5.976 secs. At a super-synchronous speed for a wind velocyt of 12 m/s, the DFIG operated for 6.5 to 8 secs and the flacuations shown at a instant 7.6335 sec to 7.634 sec. In all the instants the steady state fluctuations with proposed IDPVC control with SLRP algorithm is considerably reduced shown in Fig. 14 and it improves the qualtiy of power.

The performance proposed IDPVC control with SLRP algorithm highly reduces the steady state flucutations in reactive power as shown in Fig. 15. It is clearly observe that the magnnitude flacuations are more with DPC control at sub-synchronous speed, synchronous and super-synchronous regions respectively. Such that, The performance of proposed IDPVC algorithm SLRP computation improved the quality of power in the steady state condition.

For sub-synchronous speed (7m/s), the DPC control has a THD of 6.5% in the stator currents which is beyond the standards. At the same speed, the THD for proposed IDPVC control with SLRP

algorithm is reduced and obtained at 4.29%, which is clearly observed in Fig. 16. For synchronous speed of 9.85 m/s, THD in stator currents is reduced by 1.05% from conventional DPC control (2.68%) to proposed IDPVC control (1.63%) which is depicted in Fig. 17. At 12 m/s (super-synchronous speed), THD in stator currents for DPC control is obtained at 1.60% to that of IDPVC control is achieved at 1.18% shown in Fig. 18. The THD is improved with SLRP computation for the proposed IDPVC controller at all the aforementioned speeds as this proposed method achieves in minimizing the real and reactive power ripples which subsequently plays a key role in reducing THD. The performance parmaeters of proposed IDPVC control SLRP computationare exclusively shown in Table2.

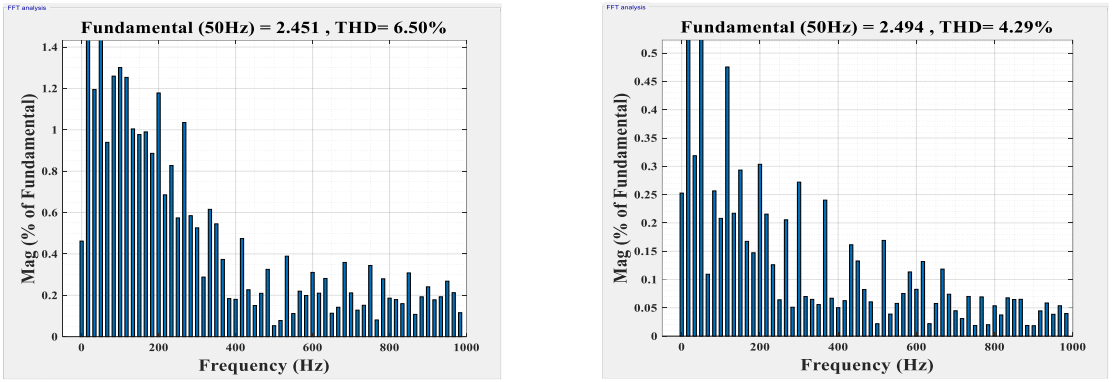

(a) (b)

Fig. 16 THD in stator currents at 7 m/s for (a) benchmark DPC control (b) proposed IDPVC control.

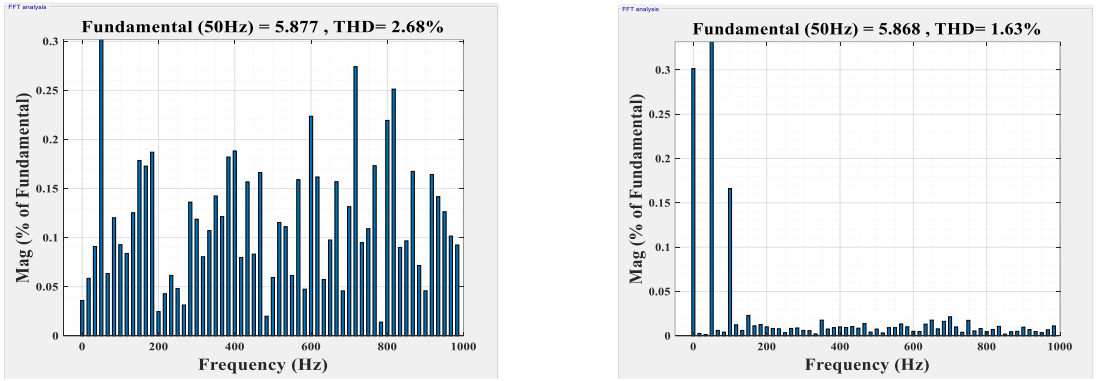

(a) (b)

Fig. 17 THD in stator currents at 9.85 m/s for (a) benchmark DPC control (b) proposed IDPVC control.

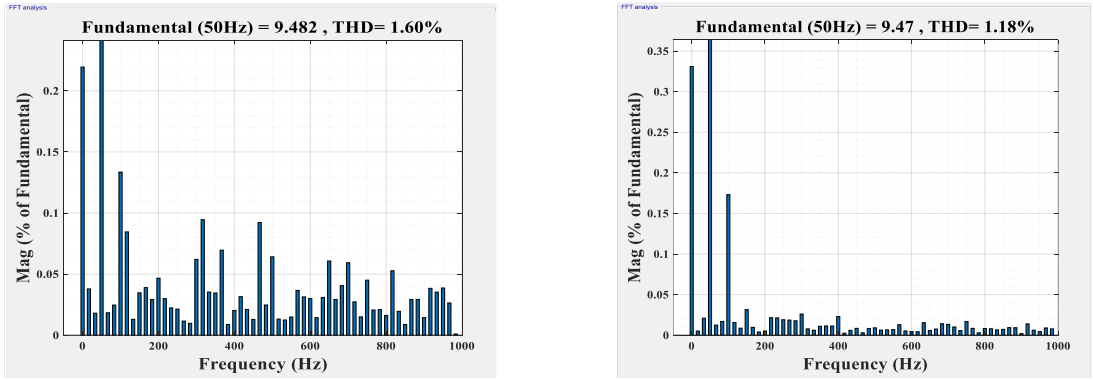

(a) (b)

Fig. 18 THD in stator currents at 12 m/s for (a) benchmark DPC control (b) proposed IDPVC control.

Table 2 The overall improved performance of IDPVC control over conventional DPC control SLRP algorithm.

Wind Speed in m/s	Real power fluctuations in steady state		Reactive power fluctuations in steady state		THD (%) in stator currents	
	Conventional DPC	Proposed IDPVC	Conventional DPC	Proposed IDPVC	Conventional DPC	Proposed IDPVC
7	125	120	160	80	6.5	4.29
9.85	150	140	160	70	2.68	1.63
12	120	110	180	80	1.60	1.18

7 Conclusion

A novel technique is proposed in this work, in order to control S-VSC interfaced DFIG at both transient and steady state response. This proposed method is based on SensorLess Rotor Position (SLRP) computation which is integrated with both direct and vector control. The efficacy of the proposed approach is compared with standard DPC control of DFIG under various wind speeds. The performance of control algorithms is tested on 3.7kW grid connected S-VSC DFIG and is compared on basis of stator real and reactive power fluctuations and total harmonic distortion in the stator currents. The results depict that, a significant reduction in steady state fluctuations for real and reactive powers at various wind speed conditions such as sub-synchronous, synchronous and super-synchronous speeds have led to an improvement in quality of power. A noteworthy enhancement in THD analysis is observed in the proposed SLRP algorithm for IDPVC control for S-VSC interfaced DFIG which ranges from 0.42%-2.21% for aforementioned wind speeds. The performance of IDPVC control is effectively controls the grid variations (LVRT) according IEGC standards. The results demonstrate that the proposed method is worthy and achieves outperforming results in evaluation the conventional method.

Appendix

System Parameters

i. Wind turbine Parameters: P_W = 6.5kW, radius= 2.018 m.
ii. DFIG parameters: P_S=3.7kW, R_S=1.32 Ω, R_r=1.708 Ω, L_S=L_r=6.832 mH, L_m=0.219 H, pole pairs=2.
iii. Mechanical parameters: J=0.1878 kg.m^2, D=0.001.
iv. Battery: 240V DC supply [21].

Intellectual Property

The authors confirm that they have given due consideration to the protection of intellectual property associated with this work and that there are no impediments to publication, including the timing to publication, with respect to intellectual property.

Funding

No funding was received for this work.

Credit Authorship Contribution Statement

R. Kalyan: Research & Investigation, Software and Simulation, Verification, Original Draft Preparation. **M. Venkatakirthiga:** Supervision, Verification. **Raja Pitchaimuthu:** Verification.

Declaration of Competing Interest

The authors hereby confirm that the submitted manuscript is an original work and has not been published so far, is not under consideration for publication by any other journal and will not be submitted to any other journal until the decision will be made by this journal. All authors have approved the manuscript and agree with its submission to "Iranian Journal of Electrical and Electronic Engineering".

References

[1] W. Leonhard, Control of electrical drives, 3rd ed. Berlin ; New York: Springer, 2001.

[2] G. Abad, J. López, M. Rodríguez, L. Marroyo, and G. Iwanski, in Doubly Fed Induction Machine: Modeling and Control for Wind Energy Generation Applications, pp. 303-361, 2011.

[3] R. Cardenas, R. Pena, S. Alepuz, and G. Asher, "Overview of control systems for the operation of DFIGs in wind energy applications," IEEE Transactions on Industrial Electronics, Vol. 60, No. 7, pp. 2776-2798, 2013.

[4] R. Datta and V. T. Ranganathan, "Variable-speed wind power generation using doubly fed wound rotor induction machine-a comparison with alternative schemes," IEEE Transactions on Energy Conversion, Vol. 17, No. 3, pp. 414–421, 2002.

[5] S. S. Murthy, B. Singh, P. K. Goel, and S. K. Tiwari, "A Comparative Study of Fixed Speed and Variable Speed Wind Energy Conversion Systems Feeding the Grid," in 2007 7th International Conference on Power Electronics and Drive Systems, 2007, pp. 736-743.

[6] L. Holdsworth, X. G. Wu, and J. B. E. N. Jenkins, "Comparison of fixed speed and doubly-fed induction wind turbines during power system disturbances," IEE Proceedings -Generation, Transmission and Distribution, Vol. 150, No. 3, pp. 343-352, 2003.

[7] E. Tremblay, S. Atayde, and A. Chandra, "Comparative study of control strategies for the doubly fed induction generator in wind energy conversion systems: A DSP-based implementation approach," IEEE Transactions on Sustainable Energy, Vol. 2, No. 3, pp. 288-299, 2011.

[8] M. V. A. Nunes, J. A. P. Lopes, H. H. Zurn, U. H. Bezerra and R. G. Almeida, "Influence of the variable-speed wind generators in transient stability margin of the conventional generators integrated in electrical grids," IEEE Transactions on Energy Conversion, Vol. 19, No. 4, pp. 692-701, 2004.

[9] R. Pena, J. C. Clare, and G. M. Asher, "Doubly fed induction generator using back-to-back PWM converters and its application to variable-speed wind-energy generation," IEE Proceedings - Electric Power Applications, Vol. 143, No. 3, pp. 231-241, 1996.

[10] S. Muller, M. Deicke, and R. W. D. Doncker, "Doubly fed induction generator systems for wind turbines," IEEE Industry Applications Magazine, Vol. 8, No. 3, pp. 26-33, 2002.

[11] A. Tapia, G. Tapia, J. X. Ostolaza, and J. R. Saenz, "Modeling and control of a wind turbine driven doubly fed induction generator," IEEE Transactions on Energy Conversion, Vol. 18, No. 2, pp. 194-204, 2003.

[12] Lie Xu and P. Cartwright, "Direct active and reactive power control of DFIG for wind energy generation," IEEE Transactions on Energy Conversion, Vol. 21, No. 3, pp. 750-758, 2006.

[13] E. Bogalecka, "Power control of a double fed induction generator without speed or position sensor," in 1993 Fifth European Conference on Power Electronics and Applications, pp. 224-228, 1993.

[14] R. Datta and V. T. Ranganathan, "A simple position-sensorless algorithm for rotor-side field-oriented control of wound-rotor induction machine," IEEE Transactions on Industrial Electronics, Vol. 48, No. 4, pp. 786-793, 2001.

[15] R. Datta and V. T. Ranganathan, "Direct power control of grid-connected wound rotor induction machine without rotor position sensors," IEEE Transactions on Power Electronics, Vol. 16, No. 3, pp. 390–399, 2001.

[16] R. Pena, R. Cardenas, J. Proboste, G. Asher, and J. Clare, "Sensorless Control of Doubly-Fed Induction Generators Using a Rotor-Current-Based MRAS Observer," IEEE Transactions on Industrial Electronics, Vol. 55, No. 1, pp. 330-339, 2008.

[17] R. Cardenas, R. Pena, J. Clare, G. Asher, and J. Proboste, "MRAS Observers for Sensorless Control of Doubly-Fed Induction Generators," IEEE Transactions on Power Electronics, Vol. 23, No. 3, pp. 1075-1084, 2008.

[18] G. D. Marques and D. M. Sousa, "Air-Gap-Power-Vector-Based Sensorless Method for DFIG Control Without Flux Estimator," IEEE Transactions on Industrial Electronics, Vol. 58, No. 10, pp. 4717-4726, 2011.

[19] A. Karthikeyan, C. Nagamani, and G. S. Ilango, "A Versatile Rotor Position Computation Algorithm for the Power Control of a Grid-Connected Doubly Fed Induction Generator," IEEE Transactions on Energy Conversion, Vol. 27, No. 3, pp. 697-706, 2012.

[20] K. Vijayakumar, N. Kumaresan, N. G. A. Gounden, and S. B. Tennakoon, "Real and reactive power control of hybrid excited wind-driven grid-connected doubly fed induction generators," IET Power Electronics, Vol. 6, No. 6, pp. 1197-1208, 2013.

[21] B. Singh and N. K. Swami Naidu, "Direct Power Control of Single VSC-Based DFIG Without Rotor Position Sensor," IEEE Transactions on Industry Applications, Vol. 50, No. 6, pp. 4152-4163, 2014.

[22] N. K. S. Naidu and B. Singh, "Sensorless control of single voltage source converter-based doubly fed induction generator for variable speed wind energy conversion system," IET Power Electronics, Vol. 7, No. 12, pp. 2996-3006, 2014.

[23] R. M. Prasad and M. A. Mulla, "A Novel Position-Sensorless Algorithm for Field-Oriented Control of DFIG With Reduced Current Sensors," IEEE Transactions on Sustainable Energy, Vol. 10, No. 3, pp. 1098–1108, 2019.

[24] R. M. Prasad and M. A. Mulla, "Mathematical Modeling and Position-Sensorless Algorithm for Stator-Side Field-Oriented Control of Rotor-Tied DFIG in Rotor Flux Reference Frame," IEEE Transactions on Energy Conversion, Vol. 35, No. 2, pp. 631–639, 2020.

[25] R. M. Prasad and M. A. Mulla, "Rotor Position-Sensorless Algorithms for Direct Power Control of Rotor-Tied DFIG," IEEE

Transactions on Power Electronics, Vol. 36, No. 6, pp. 6213–6217, 2021.

[26] R. Kalyan, V. Murali, and R. Pitchaimuthu, “Coordinate Control of Grid Power, Battery SoC and LVRT Protection in Single VSC Tied DFIG,” Distributed Generation & Alternative Energy Journal, pp. 587-608, 2022.

[27] H. Chojaa et al., "A Novel DPC Approach for DFIG-Based Variable Speed Wind Power Systems Using DSpace," IEEE Access, Vol. 11, pp. 9493-9510, 2023.

[28] B. Hu, H. Nian, J. Yang, M. Li and Y. Xu, "High-Frequency Resonance Analysis and Reshaping Control Strategy of DFIG System Based on DPC," IEEE Transactions on Power Electronics, Vol. 36, No. 7, pp. 7810-7819, 2021.

[29] S. Mondal and D. Kastha, "Input Reactive Power Controller With a Novel Active Damping Strategy for a Matrix Converter Fed Direct Torque Controlled DFIG for Wind Power Generation," IEEE Journal of Emerging and Selected Topics in Power Electronics, Vol. 8, No. 4, pp. 3700-3711, 2020.

[30] J. Mohammadi, S. Vaez-Zadeh, S. Afsharnia, and E. Daryabeigi, “A Combined Vector and Direct Power Control for DFIG-Based Wind Turbines,” IEEE Transactions on Sustainable Energy, Vol. 5, No. 3, pp. 767–775, 2014.

[31] http://niwe.res.in/NIWE_OLD/Hindi/Docu/Wind_grid_code_for_Ind.

[32] http://www.cercind.gov.in/2016/orders/420_mp_2014.pdf.

R. kalyan received the bachelor’s degree in Electrical and Electronics Engineering from BVRIT affiliated to JNTUH in 2010, and the master’s degree in Power engineering from SICET affiliated to JNTUH in 2014 respectively. He is currently pursuing as Ph.D. Scholar (2016) at the Department of Electrical and Electronics Engineering, National Institute of Technology, Tiruchirapalli. His research areas include renewable energy sources, power converters and battery storage systems.

V. Murali completed her B.E. in Electrical and Electronics Engineering and M.Tech. in Power Systems in 2000 and 2004 respectively. She is currently working as a Professor at the EEE department of the National Institute of Technology Tiruchirappalli India and has a total of eighteen years of teaching experience. She is with NITT since 2006 and has published 45 – international journal and conference publications of IEEE and Springer. She is a reviewer for many reputed journals. She has guided many UG and PG projects. She has also guided 3 Ph.D.s and 1 M.S. (by research). She is senior IEEE member and Fellow of Institution of Engineers India. Her areas of interest are Power Systems, Distributed Generation and Micro-grids and High Voltage DC Transmission.

P. Raja obtained his M.Tech degree in Energy Systems from Indian Institute of Technology Madras, Chennai in 2002 and PhD degree from National Institute of Technology, Tiruchirappalli in 2013. He is presently an Associate Professor in the Department of Electrical and Electronics Engineering at National Institute of Technology, Tiruchirappalli at India where he has been since 2006. His field of interest is design and development of controllers for power converters used in solar and wind energy conversion systems. He also does research in the development of protection schemes for transmission and distribution systems. He is a Senior Member in IEEE, life member of ISTE and Institution of Engineers (India).